Inertial-Convective Subrange Estimates of Thermal Variance Dissipation Rate from Moored Temperature Measurements

YANWEI ZHANG

State Key Laboratory of Marine Geology, Tongji University, Shanghai, China

JAMES N. MOUM

College of Oceanic and Atmospheric Sciences, Oregon State University, Corvallis, Oregon

(Manuscript received 21 October 2009, in final form 18 June 2010)

ABSTRACT

A procedure for estimating thermal variance dissipation rate χ_T by scaling the inertial-convective subrange of temperature gradient spectra from thermistor measurements on a Tropical Atmosphere Ocean (TAO) equatorial mooring, maintained by NOAA's National Data Buoy Center, is demonstrated. The inertial-convective subrange of wavenumbers/frequencies is contaminated by the vertical motion induced by the pumping of the surface float by surface gravity waves through the local vertical temperature gradient. The uncontaminated signal can be retrieved by removing the part of the measured signal that is coherent with the signal induced by surface gravity waves, which must be measured independently. An estimate of χ_T is then obtained by fitting corrected spectra to theoretical temperature gradient spectra over the inertial-convective subrange ($0.05 < f < 0.5$ Hz); this estimate is referred to as χ_T^{IC}. Here χ_T^{IC} was calculated over 120-min intervals and compared with estimates of χ_T^o determined by scaling temperature gradient spectra at high wavenumbers (viscous-convective and viscous-diffusive subranges). Large differences up to a factor of 20 and of unknown origin occur infrequently, especially when both background currents and vertical temperature gradients are weak, but the results herein indicate that 75% of the data pairs are within a factor of 3 of each other. Tests on 15-, 30-, 60-, 120-min intervals demonstrate that differences between the two methods are nearly random, unbiased, and less than estimates of natural variability determined from unrelated experiments at the same location. Because the inertial-convective subrange occupies a lower-frequency range than is typically used for turbulence measurements, the potential for more routine measurements of χ_T exists. The evaluation of degraded signals (resampled from original measurements) indicates that a particularly important component of such a measurement is the independent resolution of the surface wave–induced signal.

1. Introduction

Experiments in the laboratory (Gibson and Schwarz 1963; Sreenivasan 1996) and in naturally occurring flows (Dillon and Caldwell 1980; Nash and Moum 1999) indicate that there is something akin to a universal form in scalar gradient spectra at high wavenumbers, although the exact form may be open to question. Batchelor (1959) and Kraichnan (1968) have offered versions that are equally plausible, while subtleties remain in defining the precise values of spectral constants and in the degree of isotropy required for the maintenance of a universal spectral form (Gargett 1985; Smyth 1999, e.g.). Despite these issues, dynamically consistent estimates of the temperature variance dissipation rate χ_T appear to be derived from scaling spectral subranges (Luketina and Imberger 2001; Nash and Moum 2002).

Recently, Moum and Nash (2009) demonstrated a novel manner of obtaining estimates of χ_T from well-resolved temperature gradient measurements on an equatorial mooring. These were obtained by scaling temperature gradient spectra in the high-wavenumber subranges: the viscous-convective and viscous-diffusive subranges shown in Fig. 1. From an analysis of temperature gradient spectra obtained from a towed body (Marlin) at lower wavenumbers, Klymak and Moum (2007) have demonstrated the feasibility of obtaining reliable estimates of turbulence quantities in the inertial-convective subrange. In this analysis, estimates of the turbulent kinetic energy

Corresponding author address: Yanwei Zhang, No. 1239 Siping Road, State Key Laboratary of Marine Geology, Tongji University, Shanghai, China 200092.
E-mail: ywzhang@tongji.edu.cn

DOI: 10.1175/2010JTECHO746.1

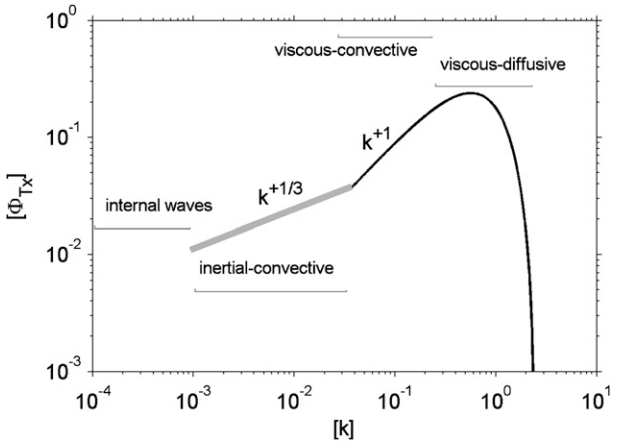

FIG. 1. Turbulence subranges in the spectrum of temperature gradient (Batchelor 1959; Dillon and Caldwell 1980; Nash and Moum 1999). Spectra and wavenumbers are nondimensionalized. The horizontal lines represent approximate frequency bandwidths of each subrange. The inertial-convective subrange is highlighted (thick gray line).

dissipation rate ϵ were compared to more direct measurements using shear probes. The towed body measurements offer a unique perspective of the turbulence in the sense that they sample the turbulence horizontally, which is the dimension we expect to have the greatest physical dimension in a vertically stratified fluid. In contrast, vertically sampled measurements as obtained from more commonly used vertical profilers sample the small dimension of the turbulence. In the vertical, it is difficult to obtain records that include the inertial-convective subrange. However, the towed records of Klymak and Moum (2007) appear to demonstrate inertial-convective subranges to surprisingly large horizontal wavenumbers (>100 m). This suggests that we may be able to use inertial-convective subrange scaling to estimate turbulence quantities from point measurements of turbulence as well, at least in the case where the fluid is rapidly advected past the point. The equatorial χpod measurements described by Moum and Nash (2009) meet this requirement.

The motivation for testing the computation of χ_T by scaling in the inertial-convective subrange is to determine how well estimates can be made using sensors with a reduced frequency range and sampling rate, in turn requiring smaller data storage capacity and potentially smaller battery capacity than we have used to date for our χpods. If the inertial-convective estimates are of sufficient quality, then we might expect that a broader range of sensors and instrumentation may be used for making direct turbulence measurements, at least in moored configurations.

The initial evaluation of temperature gradient spectra from χpods that included a motion package (three linear accelerometers) indicated that, while vortex-induced vibrations caused by the interaction of the mean current with the mooring cable had no detectable effect on measured temperature gradient spectra, wave-induced motions of the cable coupled to a surface float were significant. These motions resulted in ±1-m cable displacements at ± 0.5 m s^{-1} cable velocities in the surface gravity wave band (roughly 2–20-s periods). The consequent contamination of the temperature gradient spectra in the surface wave band was shown to be due to the vertical motion of the sensor through the vertical temperature gradient [quantified as $T_t = w_c T_z$, where T_t is the measured temperature gradient at a point (this is measured as an analog time derivative), w_c is the vertical velocity at that point on the cable, and T_z the local vertical temperature gradient]. Fortunately, viscous-convective and viscous-diffusive subranges were unaffected and reasonable estimates of χ_T were obtained. However, the surface wave–induced signal directly affects the inertial-convective subrange. Hence, this contamination must be removed prior to spectral scaling.

In this paper, we first demonstrate that the contaminating wave signal can be removed spectrally through the computation of the coherence spectrum between measured and surface wave–induced signals that are observed directly and independently. To evaluate the combined effectiveness of the removal scheme and the viability of the inertial-convective subrange estimate, we compare χ_T estimates made from high-wavenumber subranges to those estimates from the inertial-convective subrange. We then incrementally degrade the measurement, first by resampling the temperature gradient and accelerations at 2 Hz (just sufficiently enough to resolve the surface waves) and then by eliminating the accelerations from the computations and using a pressure signal to infer vertical motions only. An evaluation of χ_T estimates from the degraded measurements is made.

This paper begins with a brief review of the measurements (section 2), followed by a description of the method used to estimate χ_T, ϵ, and K_T from scalar gradient spectra (section 3), including the particular problem of removing the part of the temperature gradient signal solely resulting from vertical pumping through a temperature gradient by surface waves (section 3c). We compare the results of inertial-convective subrange estimates to those estimated from high-wavenumber scaling of the spectra in section 4, and then address the issue of how well we might quantify the turbulence with less well-resolved measurements by suitably degrading the signal (section 5). We close with a set of conclusions (section 6).

2. Measurements

In September 2005, three χpods were deployed on National Oceanic and Atmospheric Administration's (NOAA's) Tropical Atmosphere Ocean (TAO) mooring at 0°, 140°W at depths of 29, 49, and 84 m. Each unit was equipped with two fast thermistors, a pressure sensor, a compass, and three orthogonally positioned linear accelerometers. Temperature (T) was sampled at 10 Hz and its time derivative (T_t) at 120 Hz. The accelerometers reveal that the χpods experience a convoluted motion, primarily resulting from surface wave pumping. The mooring's surface float transmits large vertical and horizontal motions induced by surface gravity waves to the mooring cable. Horizontal motions are attenuated with increasing depth, while the vertical motions in the surface gravity wave band (0.05–1 Hz) are constant with depth to at least 84 m.

A complete description of χpod and of this particular deployment is given by Moum and Nash (2009). Corresponding background current speed (U_s) in the earth's coordinate system was calculated from current components ($U_s = \sqrt{U^2 + V^2}$) measured using point Doppler current meters on the mooring. The flow speed (u) past a sensor requires the measurement of the current components (U^B, V^B, W^B) in the χpod coordinate system transformed from the earth's coordinate system as well as the χpod motion itself (u_c, v_c, w_c), computed through time integration of accelerometer measurements. Thus, $u = [(u_c - U^B)^2 + (v_c - V^B)^2 + (w_c - W^B)^2]^{1/2}$. The transformations to correctly obtain u and a complete analysis of the motion of χpod on the TAO mooring using a full inertial navigation system is described by A. Perlin and J. N. Moum (2010, unpublished manuscript).

Using the horizontal component of the temperature gradient T_x computed from the time derivative T_t via Taylor's frozen flow hypothesis $T_x = T_t/u$, Moum and Nash (2009) computed χ_T from the viscous-convective and viscous-diffusive subranges of the temperature gradient spectra on 1-s intervals. These computations form the basis for comparison to the inertial-convective estimates made here.

The local vertical gradient of temperature T_z was derived by fitting temperature to depth over many surface wave periods. Two-minute-averaged fits were used to compute T_z in this paper, the same as in the analysis of Moum and Nash (2009).

3. Methodology

a. Definitions

To estimate χ_T from either viscous-convective and viscous-diffusive subranges (Moum and Nash 2009) or from inertial-convective subranges (herein), we use an iterative procedure described by Moum and Nash (2009) that requires an estimate of the turbulent kinetic energy dissipation rate of ϵ; χ_T is defined as

$$\chi_T = 6D_T \int_0^\infty \Phi_{T_x}(f)\, df, \tag{1}$$

where D_T is the thermal diffusivity and $\Phi_{T_x}(f)$ is the frequency (f) spectrum of T_x.

From Osborn and Cox (1972), the eddy diffusivity for heat (K_T) can be estimated as

$$K_T = \frac{\chi_T}{2T_z^2}. \tag{2}$$

Alternatively, a local balance of turbulent kinetic energy (TKE) between shear production, buoyancy production, and ϵ leads to another estimate of eddy diffusivity for density (K_ρ),

$$K_\rho = \Gamma\epsilon/N^2, \tag{3}$$

where N^2 is the local squared buoyancy frequency, and we assume $\Gamma = 0.2$ is a constant mixing efficiency (Osborn 1980). If $K_T = K_\rho$, then

$$\epsilon_\chi = \frac{N^2\chi_T}{2\Gamma T_z^2}. \tag{4}$$

Here, we use ϵ_χ to indicate that the TKE dissipation rate estimated from thermal variance dissipation rate χ_T.

To avoid the wave-induced contamination between 0.05 and 1 Hz, Moum and Nash (2009) estimated χ_T from windowed and detrended 1-s records. Such short records permitted the evaluation of temperature gradient spectra in viscous-convective and viscous-diffusive subranges. We use high-wavenumber estimates of χ_T, ϵ_χ, and K_T in the present analysis and refer to them here as χ_T^o, ϵ_χ^o and K_T^o (Table 1).

TABLE 1. Summary of notation used in this paper for thermal variance dissipation rate χ_T. Corresponding turbulent kinetic energy dissipation rate (ϵ_χ) and eddy diffusivity (K_T) are designated similarly.

	Subrange	Sample rate (Hz)	w_c computed from
χ_T^o	Viscous	120	Accelerometer
χ_T^{IC}	Inertial-convective	120	Accelerometer
χ_T^{IC1}	Inertial-convective	2	Accelerometer
χ_T^{IC0}	Inertial-convective	2	Pressure

b. Inertial-convective subrange

The temperature gradient spectrum Φ_{T_x} in the inertial-convective subrange (Batchelor 1959) is defined as

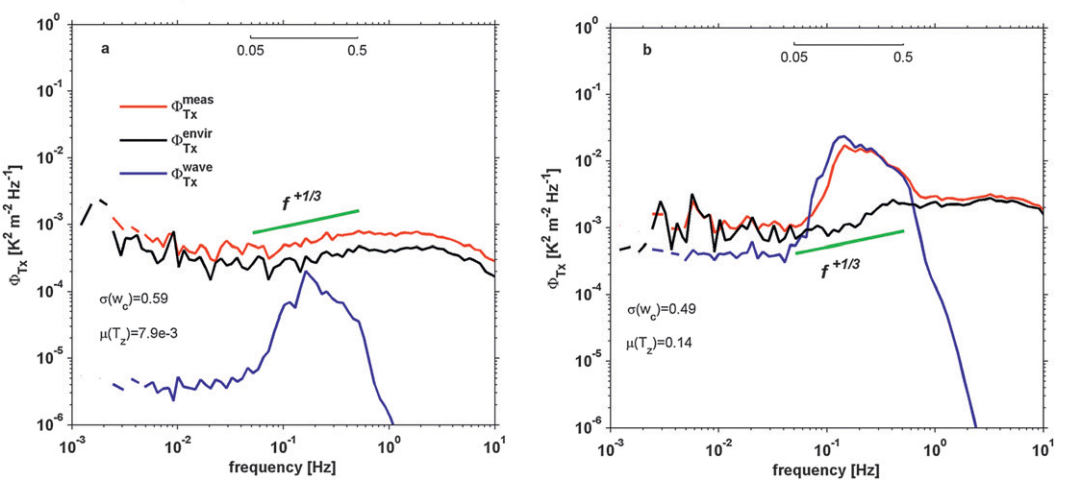

FIG. 2. Spectra of T_x ($\Phi_{T_x}^{meas}$; red line), $w_c T_z/u$ ($\Phi_{T_x}^{wave}$; blue line), and corrected spectra of T_x ($\Phi_{T_x}^{envir}$; black line). (a) From 0100 to 0300 LT 11 Oct at 29 m. (b) From 1500 to 1700 LT 1 Oct at 29 m. The bandwidth of the inertial-convective fit ($0.05 < f < 0.5$ Hz) is shown as the green line with slope $f^{1/3}$.

$$\Phi_{T_x}(k) = C_T \chi_T \epsilon^{-1/3} k^{1/3}, \tag{5}$$

where $C_T \approx 0.4$ (Sreenivasan 1996) is the Obukhov–Corrsin constant.

With wavenumber $k = 2\pi f/u$, the equivalent frequency spectrum is

$$\Phi_{T_x}(f) = 2\pi C_T \chi_T \epsilon^{-1/3} (2\pi f/u)^{1/3} u^{-1}. \tag{6}$$

Using Eq. (4), Eq. (6) can be rewritten in terms of χ_T as

$$\Phi_{T_x}(f) = (2\pi)^{4/3} C_T \left(\frac{2\Gamma T_z^2}{N^2}\right)^{1/3} \chi_T^{2/3} u^{-4/3} f^{1/3}, \tag{7}$$

or in terms of ϵ_χ as

$$\Phi_{T_x}(f) = (2\pi)^{4/3} C_T \frac{2\Gamma T_z^2}{N^2} \epsilon_\chi^{2/3} u^{-4/3} f^{1/3}. \tag{8}$$

The spectrum shown in Fig. 2a, which is unaffected by wave-induced contamination, suggests that the frequency range $0.05 < f < 0.5$ Hz is dominated by inertial-convective motions. We fit observed spectra to Eq. (7) over this frequency range, minimizing e over the inertial-convective subrange, where

$$e = \int_{f_1}^{f_2} [\log_{10}(\Phi_{T_x}^{envir}/\Phi_{T_x}^{theory})]^2 df, \tag{9}$$

$f_1 = 0.05$ Hz, and $f_2 = 0.5$ Hz; $\Phi_{T_x}^{theory}$ is represented by Eq. (7) and $\Phi_{T_x}^{envir}$ represents the uncontaminated, observed spectrum. The resulting estimates are designated χ_T^{IC}, ϵ_χ^{IC}, and K_T^{IC} (Table 1). However, because in most cases (e.g., Fig. 2b) the inertial-convective range is influenced by motions induced by surface gravity waves, we must first attempt to minimize the effects of surface wave contamination.

c. *Removal of surface wave contamination*

Measurements of T_t on a mooring cable that is vertically pumped by surface waves via the mooring's float contain a contribution resulting from that motion through the vertical temperature gradient T_z (Moum and Nash 2009). The vertical cable speed is deduced by integrating the vertical component of acceleration and denoted as w_c. In the case of these particular measurements, surface wave contamination is apparent over the frequency band $0.05 < f < 1$ Hz (Fig. 2). The measured signal T_t^{meas} can be considered to be the sum of the environmental signal T_t^{envir} plus a contribution from the surface wave–induced pumping T_t^{wave},

$$T_t^{meas} = T_t^{envir} + T_t^{wave} = T_t^{envir} + w_c T_z. \tag{10}$$

Using Taylor's frozen flow hypothesis, the spatial derivative of temperature is

$$T_x^{meas} = \frac{1}{u} T_t^{meas} = \frac{1}{u} T_t^{envir} + \frac{w_c}{u} T_z. \tag{11}$$

We remove that part of the measured signal that is coherent with the vertically pumped signal to recover our estimate of the true environmental signal (Levine and Lueck 1999),

$$\Phi_{T_x}^{envir} = \Phi_{T_x}^{meas}(1 - \gamma), \tag{12}$$

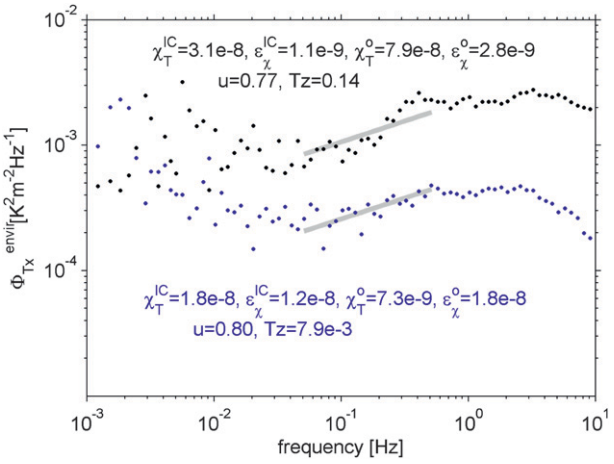

FIG. 3. Details of the corrected spectra shown in Fig. 2. Fits of the inertial-convective subrange over the interval $0.05 < f < 0.5$ Hz are shown (gray lines). Mean values of u and T_z over each 120-min interval are noted. The fits yield the estimates χ_T^{IC} and $\epsilon_\chi^{\mathrm{IC}}$. The corresponding 120-min-averaged values of χ_T^o and ϵ_χ^o derived from the 1-s estimates made by Moum and Nash (2009) are noted.

where

$$\gamma = \frac{\left|\Phi_{T_x}^{\mathrm{cross}}\right|^2}{\Phi_{T_x}^{\mathrm{meas}}\Phi_{T_x}^{\mathrm{wave}}} \tag{13}$$

represents the coherence spectrum of the signal between the measured and surface wave–induced signal. Here, $\Phi_{T_x}^{\mathrm{cross}}$ is the cross-spectrum of T_x^{meas} and $w_c T_z/u$.

Two examples are shown in Fig. 2. In Fig. 2a, T_z is relatively small and the surface wave contamination of the measured spectrum is nonexistent. In the frequency band $0.05 < f < 0.5$ Hz, the slope of the measured spectrum is close to $f^{1/3}$, which is expected for the inertial-convective subrange [Eq. (6)]. In contrast, the spectrum shown in Fig. 2b coincides with larger T_z, and the surface wave pumping dominates the spectrum in the surface gravity wave band, $0.05 < f < 1$ Hz. However, correction of the measured spectrum via Eq. (12) results in a spectrum similar to that in Fig. 2a.

Inertial-convective subrange fits to the corrected spectra in Figs. 2a,b are shown in Fig. 3. Both χ_T^{IC} and $\epsilon_\chi^{\mathrm{IC}}$ were estimated from 120-min spectral averages. These were compared to the 120-min averages of χ_T^o and ϵ_χ^o in Fig. 3. Differences are about a factor of 2–3.

4. Statistical comparison

To assess the skill of the combination of surface wave contamination removal and the inertial-convective subrange fitting procedure in estimating χ_T^{IC}, $\epsilon_\chi^{\mathrm{IC}}$, and K_T^{IC},

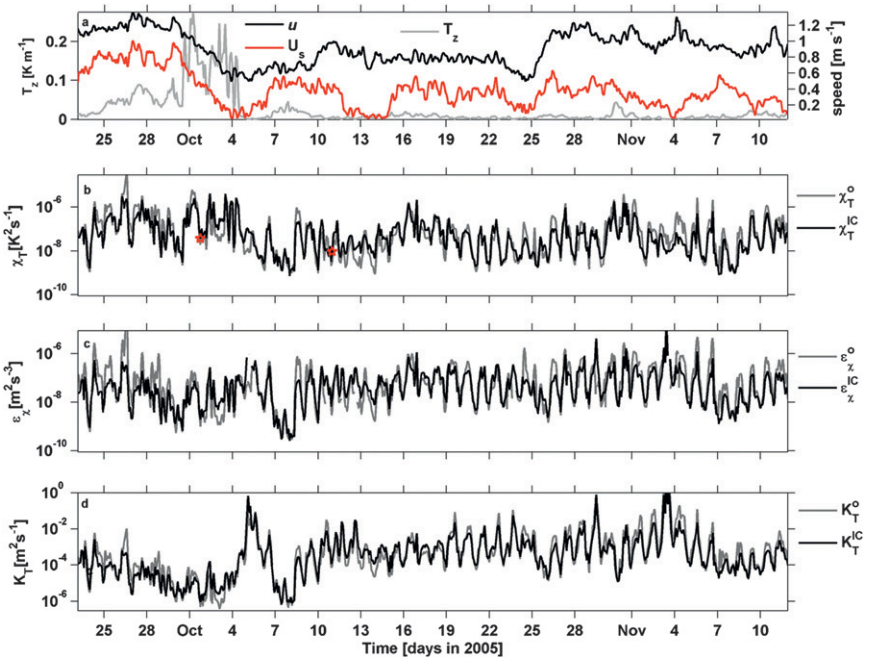

FIG. 4. Time series of (a) T_z (gray), flow speed past the thermistor u (black), and background current speed U_s (red), (b) χ_T, (c) ϵ_χ, and (d) K_T. These represent 120-min averages (T_z, χ_T^o, ϵ_χ^o, and K_T^o) and inertial-convective subrange spectral fits over 120-min intervals to obtain χ_T^{IC}, from which $\epsilon_\chi^{\mathrm{IC}}$ and K_T^{IC} are derived. Times corresponding to the examples shown in Figs. 2 and 3 are shown (red stars).

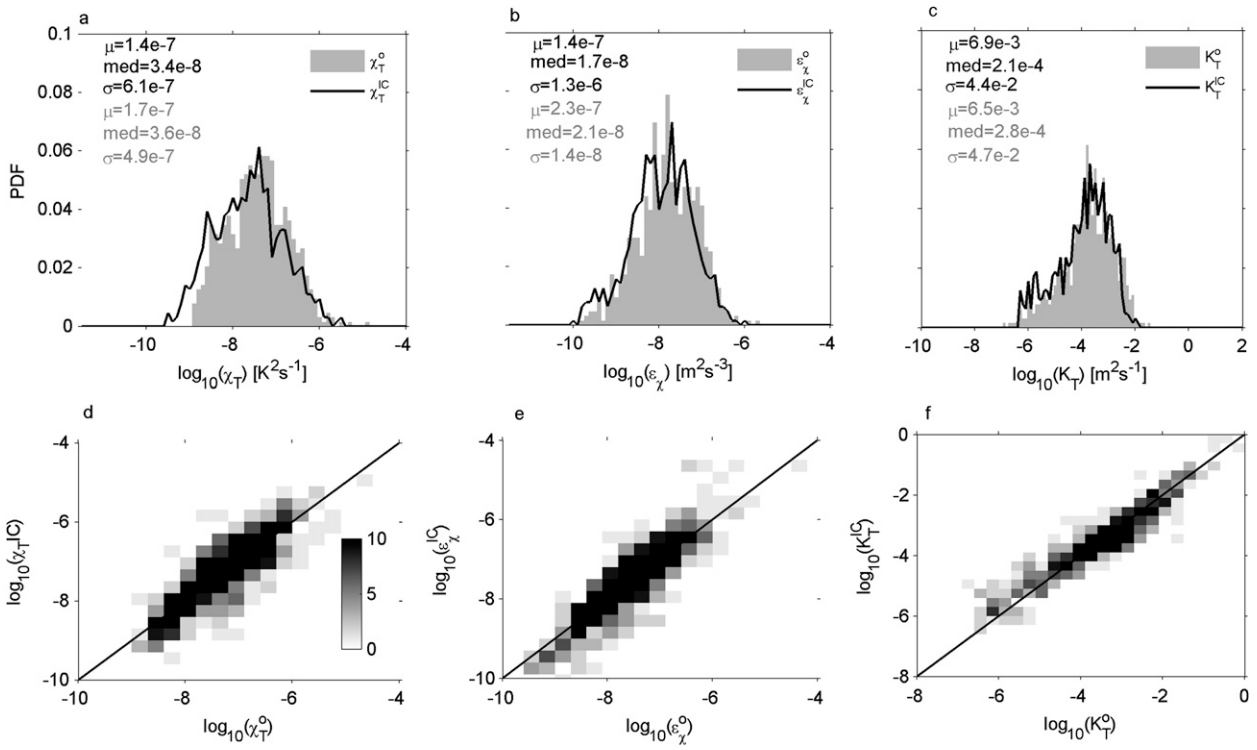

FIG. 5. Statistical comparison of results estimated from 120-min averages from high-wavenumber turbulence subrange estimates (Moum and Nash 2009) and inertial-convective subrange spectral estimates (120 min). Probability distributions of (a) χ_T, (b) ϵ_χ, and (c) K_T. The mean value μ, the median, and the standard deviation σ of each distribution are noted in the legends. Two-dimensional histogram of the two estimates of (d) χ_T, (e) ϵ_χ, and (f) K_T, respectively. In (d) the percentage of data pairs that are within factors of 2, 3, 5, and 10 of each other are listed.

we compare them to averaged values of χ_T^o, ϵ_χ^o, and K_T^o from the 6-week records obtained at 0°, 140°W and 29-m depth in September–October 2005 (Fig. 4). The initial comparison is on 120-min interval estimates. Two distinct trends appear in Fig. 4b and they are detected by both χ_T^o and $\chi_T^{\rm IC}$. The diurnal cycle of upper equatorial ocean mixing is clear, as is a longer period trend associated with changes in stratification and currents at 29 m. There also exist periods of time, however, when significant and prolonged differences between χ_T^o and $\chi_T^{\rm IC}$ occur. Large differences of up to a factor of 20 occur under various magnitudes of u, U_s, and T_z (Figs. 4a,b).

We have been unable to diagnose the precise reasons for these discrepancies. However, one source of contamination that may adversely enhance the high wavenumbers, while perhaps not affecting the inertial-convective subrange of wavenumbers, may occur when mean flow speeds are low, that is, much smaller than cable speeds. In this case, the pumping of the χpod and cable will create a wake that is not flushed from the measurement volume by the mean current. This will directly affect high wavenumbers, while larger scales may be advected through undisturbed. In this case, $\chi_T^{\rm IC}$ will provide a better estimate. This may explain some cases where $\chi_T^{\rm IC} \ll \chi_T^o$ and U_s is small, such as the periods near 26 October and 4 November, which are associated with minima in U_s (Fig. 4b).

Another potential contaminant is of a biological nature, which has concerned us from the beginning of the project. Growth of biology, including bacterial films on the thermistor, will also reduce the heat transfer rate from the fluid to the thermistor, thereby slowing the thermistor's response. This will attenuate the thermistor's high-wavenumber (fast) response but not the low-wavenumber (slow) response. Although we have taken considerable effort to minimize biological contamination, by making sensors using copper and adding protectors (Moum and Nash 2009), it is possible that this may occur on some deployments, and we continue to monitor the frequency response between beginning and ending deployments as a check. The attenuation ought to produce the result $\chi_T^o \ll \chi_T^{\rm IC}$.

A statistical comparison derived from the full 6-week record that includes, but deemphasizes, the few examples of poor agreement, indicates no significant bias between the two estimates χ_T^o and $\chi_T^{\rm IC}$ when computed over 120-min intervals (Fig. 5). Median values are within 40% of each other (Figs. 5a,d). Mean values differ by

about a factor of 2, dominated by the relatively few very high values of χ_T^o that are not predicted by χ_T^{IC}. This result is similarly reflected in comparative estimates of ϵ_χ (Figs. 5b,e) and K_T (Figs. 5c,f). A summary of the results in Fig. 5d indicates that 51% of the $[\chi_T^o, \chi_T^{IC}]$ pairs are within a factor of 2 of each other, 75% are within a factor of 3, 91% are within a factor of 5, and virtually all of the estimates (98%) are within a factor of 10.

We know that the natural variability of turbulence can contribute to variations in χ_T by several orders of magnitude on times shorter than 120 min. When this happens the spectrum of T_x does not represent a stationary process, in violation of Batchelor's original assumptions, so the form given by Eq. (7) is not necessarily representative. As a test, we recomputed χ_T^o and χ_T^{IC} on time intervals of 15, 30, and 60 min. A statistical comparison indicates similar agreement at all intervals (Fig. 6). In all cases, approximately 90% of the data pairs are within a factor of 5 of each other. As a point of reference for the degraded results discussed in section 5, the kurtosis (K) of the ratio χ_T^{IC}/χ_T^o for the four different time intervals of 15, 30, 60, and 120 min is 3.4, 3.3, 3.2, and 3.1, respectively. Here, kurtosis of the normal distribution is 3. Distributions that are more outlier prone than the normal distribution have kurtosis greater than 3.

5. Estimates from degraded measurements

The χpod measurements were intended to resolve the full spectrum of temperature gradient (within the limitations of the thermistors). To do this, the data were sampled at 120 Hz, and dynamic response corrections derived from separate field calibration measurements were then applied to spectra prior to scaling in the high-wavenumber turbulence subranges (Moum and Nash 2009). As well, the χpod motion was measured to determine both vibrational contamination and cable speeds. However, if the inertial-convective subrange scaling is adequate, then we may be able to accept lower data rates and less-well-resolved motion measurements. We test this first by subsampling the temperature gradient and accelerometer signals at 2 Hz (thus at least ensuring resolution of the surface wave–induced motion), and using the cable speed determined by integration of the subsampled accelerometer record. We then suppose that we have no accelerometer, and determine the cable speeds through differentiation of the pressure record on the χpod. This final test means that u_c and v_c are not determined (and set to 0 in our computation). However, an estimate of w_c is still available, which is essential for

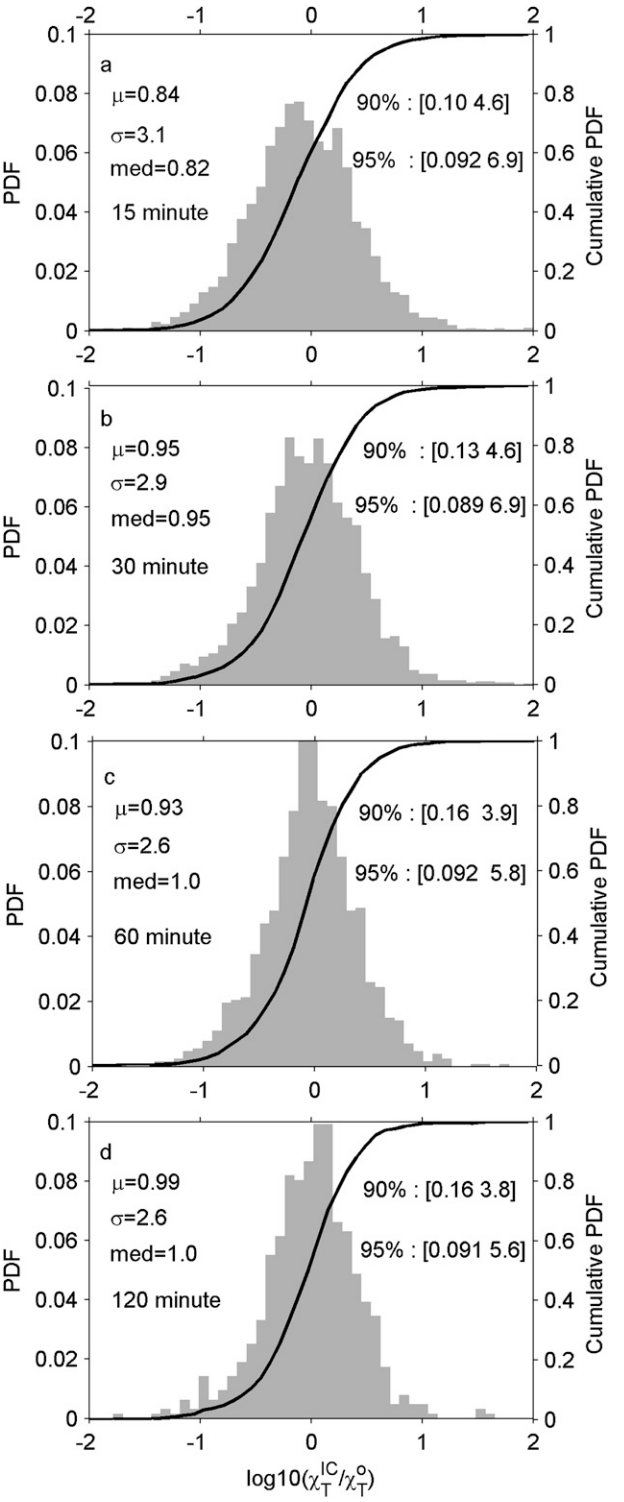

FIG. 6. Distributions of the ratio of the two estimates of χ_T computed for the intervals (a) 15, (b) 30, (c) 60, and (d) 120 min. Mean value μ, standard deviation σ, and median value "med" are given; the percentage of data pairs that are within factors of 2, 3, 5, and 10 of each other are listed in each panel.

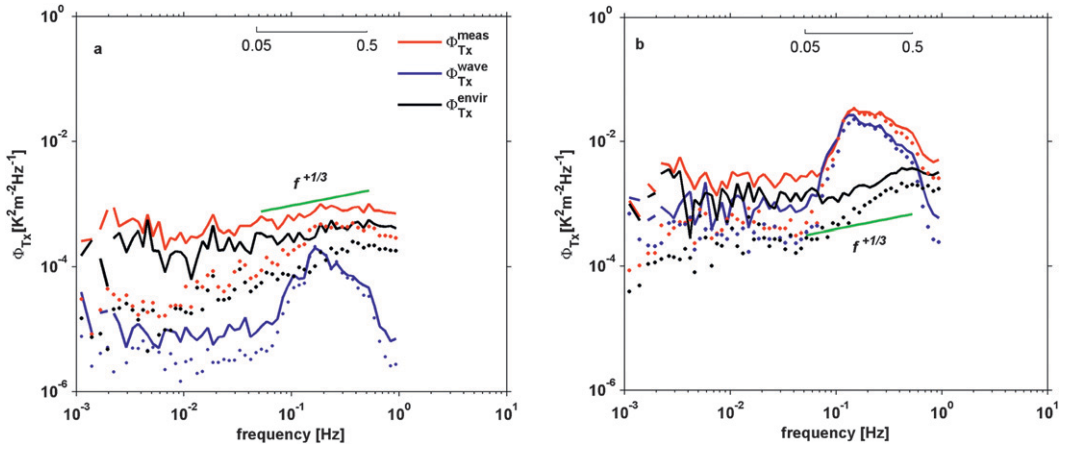

FIG. 7. (a),(b) Spectra of resampled data at 29-m depth from the periods shown in Figs. 2 and 4. The resampled data using the integrated accelerometer record to compute u_c, v_c, w_c (solid lines) and the resampled data using the differentiated pressure record to compute w_c (dotted lines). Spectra of T_x (red line), $w_c T_z/u$ (blue line), and the corresponding corrected spectra of T_x (black line). The bandwidth of the inertial-convective fit ($0.05 < f < 0.5$ Hz) is also shown as is the green line with slope $f^{1/3}$.

removal of the surface wave–induced contamination of Φ_{T_x}.

First, the records of temperature gradient (T_t) and acceleration (A_c^x, A_c^y, $A_c^z - xyz$ coordinates in the χpod body reference frame), originally sampled at 120 Hz, were filtered at 0.75 Hz and resampled at 2 Hz. Spectra corresponding to the measured temperature gradient signal and the vertically pumped signal were computed (Fig. 7), and the environmental signal was recovered via Eq. (12). Then the procedure to compute χ_T by scaling the inertial-convective subrange from Eq. (7) was applied. Resultant spectra are shown in Fig. 7 as solid lines. The results from this trial are designated as χ_T^{IC1}, ϵ_χ^{IC1}, and K_T^{IC1} (Table 1).

The procedure was then repeated with the assumption that no accelerometer was available to compute cable speeds. In this case, we estimate w_c from the depth record derived from the χpod's pressure signal $w_c = dz/dt$, but we now have no means of estimating u_c and v_c. The spectra are shown as dotted lines in Fig. 7. The results from this trial are designated as χ_T^{IC0}, ϵ_χ^{IC0}, and K_T^{IC0} (Table 1).

Estimates of χ_T, ϵ_χ, and K_T from the degraded signals are compared as time series in Fig. 8. We first consider χ_T^{IC1} (blue trace in Fig. 8b). Both long-term trends and the diurnal cycle of mixing in the upper equatorial ocean are reproduced. However, the distribution of the ratio χ_T^{IC1}/χ_T^o (Fig. 9a) shows that, in comparison to that of χ_T^{IC}/χ_T^o (Fig. 6d), σ is larger (cf. 2.6 –3.2); the median is significantly less than 1; and there is a significant number of outliers, predominantly at high values, as noted by the distribution kurtosis $K = 4.6$, which is considerably larger than 3. For comparison, 82% of the data pairs are within a factor of 5 of each other.

The more seriously degraded signal χ_T^{IC0} occasionally severely overestimates χ_T^o for extended periods,

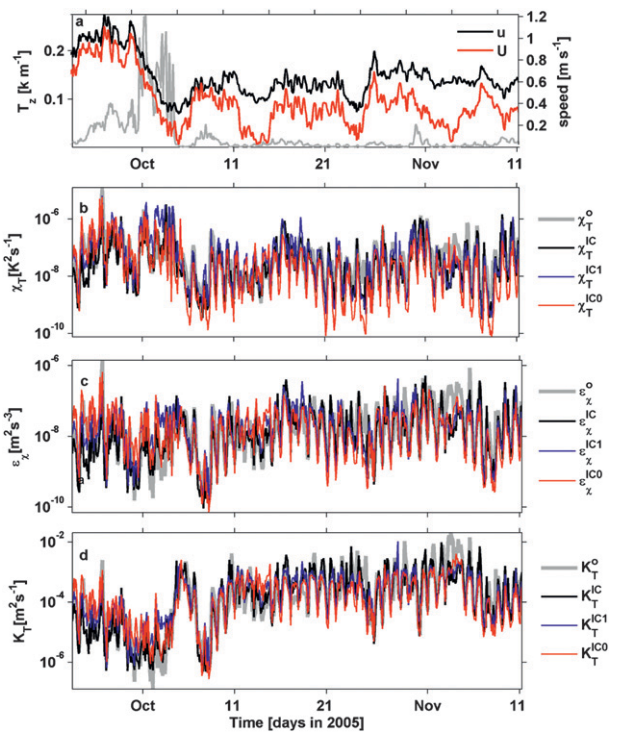

FIG. 8. As in Fig. 4, including estimates made from the degraded data. The resampled data using accelerometers to compute w_c (blue line), and results from the resampled data without accelerometers (red line). (a) Local T_z, (b) χ_T, (c) ϵ_χ, and (d) K_T.

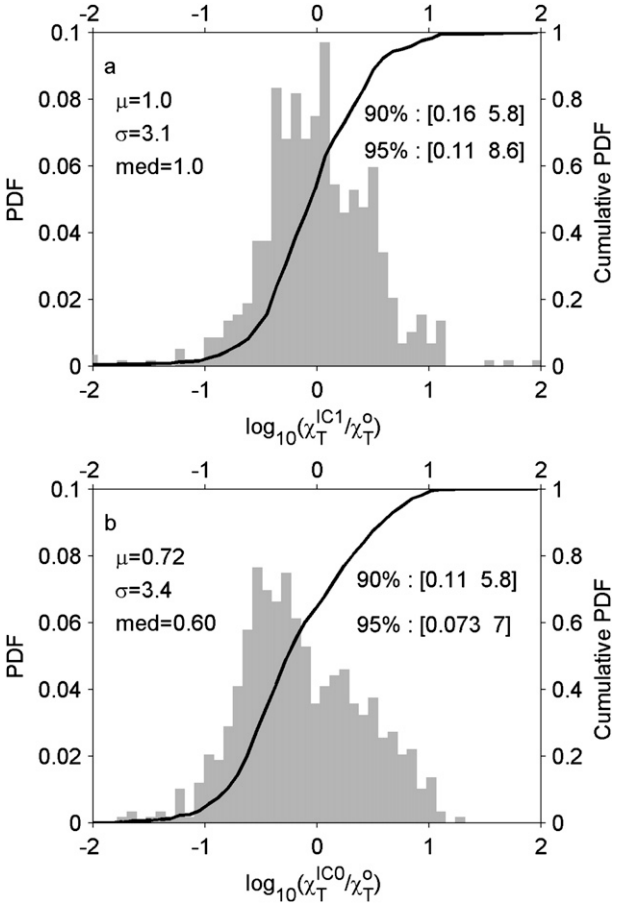

FIG. 9. As in Fig. 6, but ratios are between results from degraded data and χ_T^o. These were computed for 120-min intervals.

particularly when U_s is small (χ_T^{IC0} is the red trace in Fig. 8b). When U_s is small, the contribution of cable velocities to u are correspondingly large. Because in this case we have no measure of u_c and v_c, our estimate of u must be low, and hence our estimate χ_T^{IC0} must be high via Eq. (7), because $\Phi_{T_x} \propto u^{-4/3}$. This is represented in the distribution of χ_T^{IC0}/χ_T^o by a significantly larger standard deviation, high values of mean and median, and the large number of outliers at high values of the ratio (Fig. 9b).

6. Conclusions

To summarize, Figs. 5a,d show that estimated values of χ_T^{IC} and χ_T^o range over four orders of magnitude during the roughly 50-day period that we have examined for the purpose of this comparison. Figure 4b shows, with some exceptions, that χ_T^{IC} and χ_T^o covary on daily and longer time scales. Mean values computed over the entire time period differ by a factor of 2 (Fig. 5a). These are weighted by the outliers because mean values of ratios differ by only 10% (Fig. 6d). It is not clear whether χ_T^{IC} or χ_T^o represents the better estimate in any single sample, although we suspect that each will, in turn, provide a better estimate under different circumstances (as noted in section 4). These distributions do not show appreciable bias between the two estimates (10% at most in comparison of means of ratios). In comparison, (Moum and Nash 2009) estimated the uncertainty in individual 1-s estimates of χ_T^o to be less than a factor of three 95% of the time. This uncertainty is largely because of uncertainty in u. Averaging to 60-s intervals reduced the uncertainty to a factor of 2.

A somewhat different assessment is indicated in Fig. 5d, where it is noted that 91% of the data pairs agree within a factor of 5, or 75% of the data pairs agree within a factor of 3. Is this good enough? One metric for comparison is to the natural variability estimated from different measurements of the same process. From an experiment at the same location in 1991 (as part of the Tropical Instability Wave Experiment), Moum et al. (1995) compared estimates of ϵ from two different turbulence profilers deployed by two different groups on two ships over the same 3.5-day period and within 11 km of each other. They concluded that the systematic bias in ϵ was less than a factor of 2, which in turn was less than the estimated cumulative uncertainty in individual estimates of ϵ. Differences in hourly averaged data pairs at identical depths were attributed to natural variability. A reanalysis of the data pairs at 75-m depth (where the tightest statistical agreement was found) reveals that 51% of the data pairs were within a factor of 2 of each other, 73% within a factor of 3, 87% within a factor of 5, and 94% within a factor of 10. The agreement at 50 m was significantly poorer.

A direct measure of natural variability in χ_T at this same location comes from A. Perlin and J. N. Moum (2010, unpublished manuscript). The χpod measurements at the same depth (60 m) on moorings separated by 9 km, and CHAMELEON (a loosely tethered turbulence profiler) profiling measurements intermediate between the two moorings, yield three sets of data pairs from a 16-day period in October–November 2008. These show that roughly 30% of the data pairs were within a factor of 2 of each other, 40% within a factor of 3, 60% within a factor of 5, and 70% within a factor of 10. These ranges are markedly larger than those between our two estimates of χ_T shown in Fig. 5d, which is due to nearly random variations. This is encouraging because as long as there is no bias between our two estimates, the natural variability that must be resolved to achieve meaningful averages is greater than the variations between the two methods of estimation.

Another consideration is the long-term variations in the turbulence caused by external forcing. This is emphasized by the demonstration of greatly enhanced mixing at the same location (0°, 140°W) associated with tropical instability waves (Moum et al. 2009), resulting in mean values of ϵ above the core of the Equatorial Undercurrent by a factor of 10 greater than any previous observations (Moum et al. 2009, their Fig. 2a). The differences in our two methods are much smaller than such large variations, permitting unambiguous detection.

The reasonable agreement between the two estimates χ_T^{IC} and χ_T^o leads us to conclude that our surface wave removal is effective. Because wave-contaminated spectral values are frequently two decades higher (e.g., Fig. 2b), we would expect a considerable bias in our estimate of χ_T^{IC} from corrected spectra. If we systematically did not remove enough of the contaminating signal, then χ_T^{IC} will be high, and if we systematically removed too much, then it will be low.

Our evaluation of the degraded signals indicates that the resolution of the wave field by both temperature sensors and independent motion sensors (all three components) is necessary. It is considerably more important to measure the motion sufficiently (wave-resolving independent estimates of w_c, u_c, and v_c are required) than to oversample the records above the wave frequencies. By a proper and independent measurement of the wave-contaminated component of the temperature gradient signal, it can be effectively removed.

Acknowledgments. This work was funded by the National Science Foundation (0424133). Yanwei Zhang was supported by the State Key Laboratory of Marine Geology and Program for Young Excellent Talents in Tongji University, as well as Open Fund of the Key Lab of Ocean Circulation and Waves from Chinese Academy of Sciences. Thanks to Mike Neeley-Brown and Ray Kreth for their technical assistance and to A. Perlin for computing help. Jonathan Nash and A. Perlin have made important contributions to this project. Comments by Emily Shroyer, Aurelie Moulin, and Uwe Stoeber on an early draft are appreciated. Constructive comments by three anonymous reviewers helped to improve this paper. The continued involvement of NOAA's National Data Buoy Center through the TAO Project Office and by the Pacific Marine Environmental Laboratory has been critical to the success of this project.

REFERENCES

Batchelor, G. K., 1959: Small-scale variation of convected quantities like temperature in turbulent fluid. *J. Fluid Mech.,* **5,** 113–139.

Dillon, T. M., and D. R. Caldwell, 1980: The Batchelor spectrum and dissipation in the upper ocean. *J. Geophys. Res.,* **85,** 1910–1916.

Gargett, A., 1985: Evolution of scalar spectra with the decay of turbulence in a stratified fluid. *J. Fluid Mech.,* **159,** 379–407.

Gibson, C. H., and W. H. Schwarz, 1963: The universal equilibrium spectra of turbulent velocity and scalar fields. *J. Fluid Mech.,* **16,** 365–384.

Klymak, J. M., and J. N. Moum, 2007: Oceanic isopycnal slope spectra. Part II: Turbulence. *J. Phys. Oceanogr.,* **37,** 1232–1245.

Kraichnan, R., 1968: Small-scale structure of a scalar field convected by turbulence. *Phys. Fluids,* **11,** 945–953.

Levine, E. R., and R. G. Lueck, 1999: Turbulence measurement from an autonomous underwater vehicle. *J. Atmos. Oceanic Technol.,* **16,** 1533–1544.

Luketina, D. A., and J. Imberger, 2001: Determining turbulent kinetic energy dissipation from Batchelor curve fitting. *J. Atmos. Oceanic Technol.,* **18,** 100–113.

Moum, J. N., and J. D. Nash, 2009: Mixing measurements on an equatorial ocean mooring. *J. Atmos. Oceanic Technol.,* **26,** 317–336.

——, M. C. Gregg, R. C. Lien, and M. E. Carr, 1995: Comparison of turbulence kinetic energy dissipation rate estimates from two ocean microstructure profilers. *J. Atmos. Oceanic Technol.,* **12,** 346–366.

——, R.-C. Lien, A. Perlin, J. D. Nash, M. C. Gregg, and P. J. Wiles, 2009: Sea surface cooling at the equator by subsurface mixing in tropical instability waves. *Nat. Geosci.,* **2,** 761–765.

Nash, J. D., and J. N. Moum, 1999: Estimating salinity variance dissipation rate from conductivity microstructure measurements. *J. Atmos. Oceanic Technol.,* **16,** 263–274.

——, and ——, 2002: Microstructure estimates of turbulent salinity flux and the dissipation spectrum of salinity. *J. Phys. Oceanogr.,* **32,** 2313–2333.

Osborn, T. R., 1980: Estimates of the local rate of vertical diffusion from dissipation measurements. *J. Phys. Oceanogr.,* **10,** 83–89.

——, and C. S. Cox, 1972: Oceanic fine structure. *Geophys. Fluid Dyn.,* **3,** 321–345.

Smyth, W. D., 1999: Dissipation range geometry and scalar spectra in sheared, stratified turbulence. *J. Fluid Mech.,* **401,** 209–242.

Sreenivasan, K. R., 1996: The passive scalar spectrum and the Obukhov-Corrsin constant. *Phys. Fluids,* **8,** 189–196.